Water vapor isotopes indicating rapid shift among multiple moisture sources for the 2018/2019 winter extreme precipitation events in Southeast China

Tao Xu[1], Hongxi Pang[1,2], Zhaojun Zhan[1], Wangbin Zhang[1], Huiwen Guo[1], Shuangye Wu[3], and Shugui Hou[1,4]

[1] Key Laboratory of Coast and Island Development of Ministry of Education, School of Geography and Ocean Science, Nanjing University, Nanjing, 210023, China

[2] Collaborative Innovation Center of Climate Change, Jiangsu Province, Nanjing, 210023, China

[3] Department of Geology, University of Dayton, Dayton, OH 45469, USA

[4] School of Oceanography, Shanghai Jiao Tong University, Shanghai, 200240, China

Correspondence: H. Pang (hxpang@nju.edu.cn) and S. Hou (shuguihou@sjtu.edu.cn)

Abstract. In the East Asian monsoon region, winter extreme precipitation events occasionally occur and bring great social and economic losses. From December 2018 to February 2019, Southeast China experienced a record-breaking number of extreme precipitation events. In this study, we analyzed the variation of water vapor isotopes and their controlling factors during the extreme precipitation events in Nanjing, Southeast China. The results show that the variations of water vapor isotopes are closely linked to the change of moisture sources. Using a water vapor d-excess weighted trajectory model, we identified five most important moisture source regions: South China, East China Sea, South China Sea, Bay of Bengal, and Continental regions (Northwest China and Mongolia). Moreover, the variations of water vapor d-excess during a precipitation event reflect rapid shifts of moisture source regions. These results indicate that rapid shifts among multiple moisture sources are important conditions for sustaining wintertime extreme precipitation events over extended periods.

1 Introduction

South China is under the influenced of the East Asian Winter Monsoon during winter with prevailing northeasterly wind. As a result, winter precipitation is significantly less than summer (Yao et al., 2015), accounting for approximately 10% of the

total annual precipitation (Wang and Feng, 2011). However, persistent extreme winter precipitation events still occur

25   occasionally (Huang et al., 2018a; Li et al., 2020a), such as the disastrous snowstorm in January 2008 (Ding et al., 2008),

which caused great losses in agriculture, transportation, and electric power facilities (Zhou et al., 2011). Such extreme events

are likely to become more frequent with global warming (Rahmostorf and Coumou, 2011; Qin et al., 2021). Therefore,

improving the understanding of the characteristics, controlling factors, and moisture sources of winter extreme precipitation

events over South China could have great scientific as well as economic significance.

30   It is well known that extreme weather events are often caused by a combination of anomalous conditions in multiple

atmospheric circulation systems (Li et al., 2019). Previous studies attributed the winter extreme precipitation events over

South China to anomalies in the Western Pacific subtropical high, the East Asian major trough, the India-Burma trough, and

the formation of the European blocking high (Wang et al., 2000; Zong et al., 2014; Ding and Li, 2017; Huang et al., 2018b).

In addition, the variation of winter precipitation was also found to be closely related to sea surface temperature over the

35   Eastern Tropical Indian Ocean and the South China Sea (Zhou et al., 2010; Li et al., 2015a). In addition to dynamic and

thermal conditions, abundant moisture supply is also an essential condition for winter extreme precipitation events (Yang et

al., 2019; Zhao et al., 2021). Therefore, exploring the moisture sources for the extreme precipitation events is a crucial part

of understanding factors controlling these events. Previous climatological studies suggest that the most important moisture

source regions for wintertime precipitation in South China were the South China Sea, western North Pacific, and the Bay of

40   Bengal (Baker et al., 2015; Sun and Wang, 2015). However, detailed information about moisture transport and source

regions of individual extreme precipitation events is largely lacking. Moreover, the large-scale atmospheric circulation

patterns are not changing significantly at short time scale, so it is difficult for climatological studies to capture the possible

rapid switching of moisture sources during an extreme precipitation event.

Stable isotopes in precipitation and water vapor ($\delta^{18}O$ and $\delta^{2}H$) are useful natural tracers for the hydrological cycle

45   (Araguás-Araguás et al., 2000; Galewsky et al., 2016). They have been used to trace moisture sources (Bonne et al., 2014;

He et al., 2016) and identify water vapor transport pathways (Tian et al., 2007; Cai and Tian, 2016). Earlier studies have

improved our understanding of the variations of stable isotopic compositions at different time scales, especially at the

monthly and daily scales. The variability of stable isotopic compositions is not only affected by local meteorological factors, such as temperature and precipitation amount (Dansgaard, 1964; Yu et al., 2015), but also by large-scale atmospheric
50   circulations (Zhou and Li, 2017; Gao et al., 2018), and sources of moisture (Peng et al., 2010; Wang et al., 2017). In addition, deuterium excess (d-excess), defined as $d = \delta^2H - 8 \times \delta^{18}O$, is influenced by the evaporative and meteorological conditions in the moisture source region (Dansgaard, 1964; Merlivat and Jouzel, 1979), and often used as an indicator for changes in relative humidity at the source region or shifts in the moisture origin (Benetti et al., 2014). Existing studies on precipitation and water vapor isotopes often used monthly and daily data, which do not have the temporal resolution needed to study
55   isotopic changes during individual precipitation events. In addition, continuous collection of precipitation isotope data through precipitation events is often difficult due to adverse weather conditions. Therefore, a continuous monitoring of water vapor isotopes at high temporal resolution (from minutely to hourly timescales) provides a feasible way to identify changes in the moisture sources during precipitation events. Moreover, compared with precipitation, water vapor responds more sensitively to changes in atmospheric circulation (Yao et al., 2018; Li et al., 2020b).

60   From December 2018 to February 2019, the joint influence of the central Pacific El Niño and East Asian Winter Monsoon quasi-biweekly oscillation led to a long period of persistent rainfall in Southeast China. The 51 accumulated rainy days had the highest regional effective precipitation since 1981 (Guo et al., 2019; Wang et al., 2020). The regional sunshine duration was only half of the normal condition with the lowest number of sunshine hours recorded since 1961 (Li et al., 2020c). This record-breaking event provided an opportunity for using stable isotopes to understand the possible causes and
65   moisture sources of winter extreme precipitation. In this study, we monitored and analyzed the stable isotopic compositions of water vapor (with hourly resolution) and precipitation during this extreme precipitation period in Nanjing, Southeast China. We utilized these high temporal resolution data to investigate the evolution of the stable isotopic compositions in water vapor during this period, and understand how event-scale isotopic variation is affected by climate factors and moisture sources during winter extreme precipitation events.

70   **2 Materials and methods**

2.1 Study site

Sampling and measurement of stable isotopes in water vapor and precipitation were carried out at the Station for Observing

Regional Processes of the Earth System of Nanjing University (SORPES-NJU, 32.12°N, 118.95°E, 55 m above sea level) on

the Xianlin Campus of the Nanjing University, about 20 km east of downtown Nanjing in Southeast China (Li et al., 2020b).

75   Nanjing is located in the lower reaches of the Yangtze River in China and has a typical subtropical monsoon climate.

Under the influence of the East Asia Monsoon, it has a strongly seasonal climate with hot and rainy summers and cold and

dry winters. In the winter (December–February, DJF), Nanjing is under the influence of the East Asian Winter Monsoon.

According to the historical meteorological data (1981–2010), the average DJF monthly precipitation is 42 mm. From

December 2018 to February 2019, affected by the continuous rainy weather, Nanjing has 46 accumulated rainy days and the

80   total accumulated precipitation is 259 mm, more than double the seasonal average of 1981–2010 (Fig. 1).

2.2 Sampling and measurement

Water vapor sampling was carried out on the roof of the SORPES-NJU two-floor building from 1 November 2012 to the

present. Data from December 2018 to February 2019 was used for this study. The stable isotopic compositions of water

vapor ($\delta^{18}O_v$ and δ^2H_v) were measured by a Picarro Wavelength Scanned Cavity Ring-Down Spectrometer (WS-CRDS,

85   model: Picarro L2120–i). We calibrated the samples against various deviations (such as memory effect, drift effect, and

concentration effect), following a set of procedures described in Gu et al., (2019) and Li et al., (2020b). We collected one

sample every 2–3 seconds, and summarized the raw data into hourly averages for this study. The instrumental uncertainties

were less than 0.2‰ for $\delta^{18}O_v$ and 1.0‰ for δ^2H_v (Gu et al., 2019).

Along with regular water vapor sampling, precipitation samples were collected on rainy days with an amount >0.1 mm

90   from September 2011 to the present. Data from December 2018 to February 2019 was used for this study. All samples were

poured into 100–ml polyethylene bottles immediately after collection. In order to avoid evaporation, all samples were

refrigerated until being analyzed. The stable isotopic compositions in precipitation ($\delta^{18}O_p$ and δ^2H_p) were measured by a

Picarro L2120–i in the Key Laboratory of Coast and Island Development of Ministry of Education. The precision of

measurements is 0.05‰ for $\delta^{18}O_p$ and 0.5‰ for δ^2H_p (Tang et al., 2015).

2.3 Trajectory weighted concentration field

In order to trace moisture source, we used the NOAA Hybrid Single Particle Lagrangian Integrated Trajectory (HYSPLIT) model and calculated backward trajectories of air masses associated with individual extreme precipitation events, using the Global Data Assimilation System (GDAS) with a spatial resolution of 1° × 1° as the background meteorological data (ftp://ftp.arl.noaa.gov/pub/archives/gdas1). Eight-day backward trajectories were calculated every one hour with the starting height of 1500 m above ground.

Based on the HYSPLIT results, we calculated the Concentration Weighted Trajectory (CWT) field at 0.5° × 0.5° resolution to establish potential source regions that influence the isotopic variability of water vapor at the study site (Salamalikis et al., 2015; Bedaso and Wu, 2020; Li et al., 2020b). The CWT (C_{ij}) was calculated with the following equation:

$$C_{ij} = \frac{\sum_{k=1}^{K} C_k \tau_{ijk}}{\sum_{k=1}^{K} \tau_{ijk}} \, , \qquad (1)$$

where (i, j) are grid indices, k is the trajectory index, K is the total number of trajectories that pass each 0.5° × 0.5° grid, C_k the concentration (d-excess) measured upon arrival of trajectory k, and τ_{ijk} the residence time of trajectory k in grid cell (i, j).

2.4 Meteorological and reanalysis data

We obtained long-term monthly mean (1981–2010) and hourly meteorological data (air temperature, precipitation amount, and relative humidity) from December 2018 to February 2019 at Nanjing meteorological station from China Meteorological Data Service Center. We also used reanalysis data, including 850 hPa zonal and meridional wind components and temperature, from the European Centre for Medium-Range Weather Forecasts (ECMWF) Copernicus Climate Data Store (https://cds.climate.copernicus.eu) and Global Precipitation Climatology Centre (GPCC) precipitation data from the NOAA Physical Sciences Laboratory (https://psl.noaa.gov/data/gridded/).

Unless explicitly noted, the anomalies for climate variables are calculated with respect to the average of 1981–2010.

3 Results

3.1 Variations of water vapor and precipitation isotopic compositions during precipitation events

Previous studies typically identified five large-scale precipitation events during the 2018/2019 winter (Li and He, 2019; Xu et al., 2019; Zhao et al., 2019): (a) December 4−11, (b) December 24−30, 2018, (c) January 7−11, (d) February 16−22, and (e) January 27−31, 2019. Figure 2 shows the hourly average $\delta^{18}O_v$ and d_v, daily average of $\delta^{18}O_p$ and d_p, and hourly air temperature, relative humidity, and precipitation amount for those five events. $\delta^{18}O_v$ varies from −23.6‰ to −12.4‰ (with an average of −18.1‰), and dv ranges from 16.3‰ to 35.9‰ (with an average of 24.6‰). $\delta^{18}O_p$ has an range from −15.5‰ to −1.3‰ and an average of −7.0‰. d_p ranges from 13.5‰ to 32.5‰, with an average of 23.6‰. Stable isotopes in precipitation and water vapor have similar variation pattern. Therefore, only high temporal resolution water vapor isotope data are used for further analysis. Based on the large-scale atmospheric circulation patterns (Fig. 3), we group these precipitation events into three classes.

The first class (including event a and b) is defined as cold air mass dominated events. The beginning of the precipitation event was characterized by the southerly wind (Fig. 3a, b) and higher temperature (Fig. 2a, b). With the invasion of the cold air mass through the majority of the event period, the study site experienced northerly wind and temperature decrease. Towards the end of the event, the site returned to southerly wind with temperature increase. Under this circulation background, the $\delta^{18}O_v$ value was generally high at the beginning, decreased significantly during the events, and gradually increased again toward the end of the events, whereas the d_v value showed the opposite trends (Fig. 2a, b). The lowest $\delta^{18}O_v$ and highest d_v values were usually observed at the lowest temperature and relative humidity. However, changes in temperature and relative humidity cannot completely explain the variation in the $\delta^{18}O_v$ and d_v values. Air temperature and relative humidity data obtained from the meteorological station only reflect the local conditions at the sampling site (He et al., 2018), and the large-scale atmospheric circulation plays a more important role.

The second class (event c and d) is defined as warm air mass dominated events. Northerly wind and low temperature occurred only at the beginning of the precipitation event, whereas the majority of the even period was characterized by southerly wind and warm temperature (Fig. 3c, d). Similar to the first class, the $\delta^{18}O_v$ value was generally high at the

beginning, decreased significantly during the events, and gradually increased again toward the end of the events (Fig. 2c).

140   However, different from the first class, both $\delta^{18}O_v$ and dv values in this class showed many more fluctuations throughout the

event (Fig. 2c, d). The lowest $\delta^{18}O_v$ and d_v values occurred at the lowest temperature and highest relative humidity, it is

significantly different from the first class.

        In addition to the above two classes, the third class (event e) is characterized by alternating cold and warm air masses.

The event started with northerly wind and low temperature, followed by southerly wind and temperature increase, and ended

145   with northerly wind and temperature decrease (Fig. 3e). The $\delta^{18}O_v$ value remained constant in the early stage until it

decreased suddenly at the end, whereas the d_v value showed great fluctuations (Fig. 2e).

3.2 Intra-event variation of water vapor isotopic compositions

Significant variations in $\delta^{18}O_v$ and d_v values of water vapor are observed within each event. We used the concentrated rainfall

period of each event and divided it into different stages (Fig. 2), based on the above three classifications and the temporal

150   patterns of variation in water vapor $\delta^{18}O_v$ and d_v.

        The first class (Fig. 2a, b) of the precipitation events can be divided into four stages. (In the last stage of event b was not

delineated because of missing data.) In stages 1 and 2, the $\delta^{18}O_v$ values continued to decrease, which was consistent with the

temperature effect (i.e. stable isotopes had a significant positive correlation with air temperature). The d_v value first

decreased (or remained stable), then increased, suggesting a gradual shift of water vapor source from ocean to land (Fig. 2a,

155   b). Generally, atmospheric water vapor from the dry and cold regions shows a more negative $\delta^{18}O$ value and relatively high

d-excess value (Uemura et al., 2008; Kostrova et al., 2020). In stage 3, the $\delta^{18}O_v$ and d_v value fluctuated without any obvious

trends as a whole, mainly due to the mixing of oceanic and inland water vapor. In stage 4, the $\delta^{18}O_v$ value continued to

decline, consistent with the rainout effect (i.e. stable isotopes continued to decrease with the increase of precipitation

amount); the d_v value was significantly lower than the stage 3 with no obvious trend, reflecting the stable influence of

160   oceanic water vapor (Fig. 2a).

        The second class (Fig. 2c, d) of the precipitation events can be divided into three stages. In stage 1, the $\delta^{18}O_v$ value

continued to decrease, consistent with the rainout effect; the d_v value continued to decrease, suggesting a shift of water vapor

source from land to ocean. In stage 2, both the $\delta^{18}O_v$ value and d_v values increased, but still lower than the initial value in

stage 1, suggesting increasing contribution of local inland water vapor in the mixture of oceanic and inland water vapor. In

165   stage 3, the $\delta^{18}O_v$ value and d_v values showed a downward trend, reflecting the continuous influence of oceanic water vapor.

The third class (Fig. 2e) of the precipitation event can be divided into two stages. The $\delta^{18}O_v$ value was stable and

relatively high in stage 1, possibly due to the influence of local inland water vapor in South China, where the air temperature

remained high, leading to enriched isotopic values. The $\delta^{18}O_v$ value started to decline in stage 2, likely caused by the rainout

effect. The d_v value is relatively high in stage 1, likely due the contribution of local inland water vapor. The rapid decrease of

170   dv in the middle may indicate the influence of oceanic water vapor. In stage 2, the d_v value decreases rapidly, reflecting the

rapid change of moisture sources, and a shift from mixed water vapor to oceanic water vapor.

4 Discussion

4.1 Moisture sources for five precipitation events

Previous studies demonstrated that seasonal variations in the stable isotopic compositions of precipitation are caused not

175   only by local meteorological conditions (Dansgaard, 1964), but also by the different moisture sources (Bonne et al., 2020).

The above analysis results show that the large-scale circulation patterns (850 hPa meridional wind and temperature) have an

important influence on the event-scale stable isotopes in water vapor, and the variation of meridional wind often corresponds

to the change of moisture source regions. Some studies indicated that the air masses could obtain specific isotopic signatures

based on the meteorological conditions in the moisture source region before reaching a given sampling site (Salamalikis et

180   al., 2015; Kostrova et al., 2020). Therefore, based on the CWT model, we calculated the d_v value concentration fields to

investigate differences among moisture source regions and water vapor transport pathways.

As seen in Fig. 4, we identified five major moisture source regions that affect the sampling site base on cluster analysis

of backward trajectories during these precipitation events: South China, East China Sea, South China Sea, Bay of Bengal,

and Continental regions (Northwest China and Mongolia). The air parcels passing areas indicated with warm colors exhibit

185   high d-excess values in the sampling site (Salamalikis et al., 2015). Trajectories passing North China, Northwest China, and

Mongolia correspond to higher d_v values in the sampling site (Fig. 4), as they are associated with relatively dry air masses

from the inland region. Moisture from other sources show lower d_v values, due to higher relative humidity at the oceanic

source regions (Fig. 4). These results clearly indicate that the changes of moisture source regions could play an important

role in the variation of water vapor isotopic compositions in winter extreme precipitation events. Our observations are in

190 good agreement with the observation of summer extreme precipitation event by Li et al., (2015b). We believe that abundant

moisture supply through multiple moisture sources is one of the necessary conditions for the 2018/2019 winter extreme

precipitation events to last for a long time.

4.2 Rapid shift of moisture sources during a precipitation event

Fig. 2 shows the variation of stable isotopic values in different stages of the precipitation events divided by vertical blue

195 dashed lines. From the above analysis, it can be seen that the intra-event variation of stable isotopic values in water vapor

was mainly controlled by the change of moisture sources. Therefore, we believe that the turning points at the blue dashed

lines reflected rapid shifts of moisture source regions. In order to verify this hypothesis, we plotted the relationship between

the d_v value and 850 hPa wind direction in the study region. Figure 5 shows that variation of the d_v value is closely related to

rapid change in the wind direction, especially near the turning point. For example, during event a (Fig. 5a), the d_v value was

200 relatively low in the early stage, and the main wind directions are easterly and southeasterly, reflecting the influence of water

vapor from the East China Sea. From the first vertical blue dashed line, the wind direction turned northerly. As a result, the

d_v value gradually increased and remained high, mainly due to the influence of water vapor transported by cold air mass

from Northwest China and Mongolia. In the later stage, the wind direction near the second vertical blue dashed line turned to

southerly and southeasterly, and the d_v value decreased due to the water vapor from the East China Sea. Therefore, the high

205 temporal resolution d_v value in water vapor can be used to identify the rapid shift of moisture source regions during the

continuous extreme precipitation process.

5 Conclusions

In this study, we presented stable isotopes in atmospheric water vapor and precipitation for five extreme winter precipitation

210 events in Nanjing, from December 2018 to February 2019. Our analyses suggest that the variations of water vapor isotope are largely influenced by the change of moisture sources. Based on the results of the CWT model, the sampling site received different proportions of water vapor from multiple sources throughout the study period, including South China, East China Sea, South China Sea, Bay of Bengal, and Continental regions (Northwest China and Mongolia). In particular, the turning points of the water vapor d-excess during a precipitation event reflected the rapid shift of moisture source regions. Our results imply that multiple moisture sources and the rapid shift among them are important conditions for sustaining extreme

215 precipitation events, especially in the relatively cold and dry winter.

Data availability. The dataset of daily water vapor $\delta^{18}O_v$ and $\delta^{2}H_v$, air temperature, water vapor concentration, relative humidity, precipitation amount, and precipitation $\delta^{18}O_p$ and $\delta^{2}H_p$ at Nanjing are available at https://data.tpdc.ac.cn/en/data/d117f51c-b47f-4bfd-9030-0c54f15067cf/.

Author contribution. Hongxi Pang and **Shugui Hou** conceived this study. Material preparation, data collection, and

220 analysis were performed by **Tao Xu, Zhaojun Zhan,** and **Wangbin Zhang**. The first draft of the manuscript was written by **Tao Xu**. **All authors** contributed to a discussion of the results.

Competing interests. The authors declare that they have no conflicts of interest.

Acknowledgements. This work was supported by the Natural Science Foundation of China (41771031, 91837102, 41830644) and the Priority Academic Program Development of Jiangsu Higher Education Institutions (PAPD). We would

225 also like to thank the NOAA Air Resource Laboratory (ARL) for providing the HYSPLIT model used in this paper.

References

Araguás-Araguás, L., Froehlich, K., and Rozanski, K.: Deuterium and oxygen-18 isotope composition of precipitation and

atmospheric moisture, Hydrol. Process., 14, 1341–1355,

https://doi.org/10.1002/1099-1085(20000615)14:8<1341::AID-HYP983>3.0.CO;2-Z, 2000.

230   Baker, A., Sodemann, H., Baldini, J., Breitenbach, S., Johnson, K., Hunen, J. V., and Zhang, P. Z.: Seasonality of westerly

moisture transport in the East Asian summer monsoon and its implications for interpreting precipitation δ^{18}O, J.

Geophys. Res.-Atmos., 120, 5850–5862, https://doi.org/10.1002/2014JD022919, 2015.

Bedaso, Z. and Wu, S. Y.: Daily precipitation isotope variation in Midwestern United States: Implication for hydroclimate

and moisture source, Sci. Total. Environ., 713, 136631, https://doi.org/10.1016/j.scitotenv.2020.136631, 2020.

235   Benetti, M., Reverdin, G., Pierre, C., Merlivat, L., Risi, C., Steen-Larsen, H. C., and Vimeux, F.: Deuterium excess in marine

water vapor: Dependency on relative humidity and surface wind speed during evaporation, J. Geophys. Res.-Atmos.,

119, 584–593, https://doi.org/10.1002/2013JD020535, 2014.

Bonne, J. L., Masson-Delmotte, V., Cattani, O., Delmotte, M., and Steen-Larsen, H. C.: The isotopic composition of water

vapour and precipitation in Ivittuut, southern Greenland, Atmos. Chem. Phys., 14, 4419–4439,

240   https://doi.org/10.5194/acp-14-4419-2014, 2014.

Bonne, J. L., Meyer, H., Behrens, M., Boike, J., Kipfstuhl, S., Rabe, B., Schmidt, T., Schönicke, L., Steen-Larsen, H. C., and

Werner, M.: Moisture origin as a driver of temporal variabilities of the water vapour isotopic composition in the Lena

River Delta, Siberia, Atmos. Chem. Phys., 20, 10493–10511, https://doi.org/10.5194/acp-20-10493-2020, 2020.

Cai, Z. and Tian, L.: Processes governing water vapor isotope composition in the Indo-Pacific region: Convection and water

245   vapor transport, J. Climate., 29, 8535–8546, https://doi.org/10.1175/JCLI-D-16-0297.1, 2016.

Dansgaard, W.: Stable isotopes in precipitation, Tellus., 16, 436–468, https://doi.org/10.3402/tellusa.v16i4.8993, 1964.

Ding, F. and Li, C.: Subtropical westerly jet waveguide and winter persistent heavy rainfall in south China, J. Geophys.

Res.-Atmos., 122, 7385–7400, https://doi.org/10.1002/2017JD026530, 2017.

Ding, Y., Wang, Z., Song, Y., and Zhang, J.: Causes of the unprecedented freezing disaster in January 2008 and its possible

250   association with the global warming, Acta. Meteorol. Sin., 66, 808–825, 2008 (in Chinese with English abstract).

Gao, J., He, Y., Masson-Delmotte, V., and Yao, T.: ENSO effects on annual variations of summer precipitation stable isotopes

in Lhasa, southern Tibetan Plateau, J. Climate., 31, 1173–1182, https://doi.org/10.1175/JCLI-D-16-0868.1, 2018.

Galewsky, J., Steen-Larsen, H. C., Field, R. D., Worden, J., Risi, C., and Schneider, M.: Stable isotopes in atmospheric water vapor and applications to the hydrologic cycle, Rev. Geophys., 54, 809–865, https://doi.org/10.1002/2015RG000512, 2016.

Gu, X., Pang, H., Li, Y., Zhang, W., and Wang, J.: Study on calibration method for atmospheric water vapor stable isotopes observed by cavity ring-down spectroscopy, Spectrosc. Spect. Anal., 39, 1700−1705, 2019.

Guo, L., Liu, B., and Zhu, C.: Extraordinary long wet spell in south of Yangtze River during 2018/2019 winter and its possible causes, Chinese. Sci. Bull., 64, 3498−3509, https://doi.org/10.1360/N972019-00357, 2019 (in Chinese with English abstract).

He, S. and Richards, K.: Stable isotopes in monsoon precipitation and water vapour in Nagqu, Tibet, and their implications for monsoon moisture, J Hydrol., 540, 615–622, https://doi.org/10.1016/j.jhydrol.2016.06.046, 2016.

He, S., Goodkin, N. F., Kurita, N., Wang, X., and Rubin, C. M.: Stable isotopes of precipitation during tropical Sumatra squalls in Singapore, J. Geophys. Res.‐Atmos., 123, 3812–3829, https://doi.org/10.1002/2017JD027829, 2018.

Huang, W., He, X., Yang, Z., Qiu, T., Wright, J. S., Wang, B., and Lin, D.: Moisture sources for wintertime extreme precipitation events over South China during 1979–2013, J. Geophys. Res.‐Atmos., 123, 6690–6712, https://doi.org/10.1029/2018JD028485, 2018a.

Huang, W., Yang, Z., He, X., Lin, D., Wang, B., Wright, J. S., Chen, R., Ma, W., and Li, F.: A possible mechanism for the occurrence of wintertime extreme precipitation events over South China, Clim. Dynam., 52, 2367–2384, https://doi.org/10.1007/s00382-018-4262-8, 2018b.

Kostrova, S. S., Meyer, H., Fernandoy, F., Werner, M., and Tarasov, P. E.: Moisture origin and stable isotope characteristics of precipitation in southeast Siberia, Hydrol. Process., 34, 51–67, https://doi.org/10.1002/hyp.13571, 2020.

Li, X., Li, J., and Li, Y.: Recent winter precipitation increase in the Middle-Lower Yangtze River Valley since the Late 1970s: A response to warming in the Tropical Indian Ocean, J. Climate., 28, 3857–3879, https://doi.org/10.1175/JCLI-D-14-00701.1, 2015a.

Li, J., Tao, T., Pang, Z., Tan, M., Kong, Y., Duan, W., and Zhang, Y.: Identification of different moisture sources through isotopic monitoring during a storm event, J. Hydrometeorl., 16, 1918–1927, https://doi.org/10.1175/JHM-D-15-0005.1, 2015b.

Li, C., Yang, H., and Zhao, J.: Combinational anomalies of atmospheric circulation system and occurrences of extreme weather/climate events, Trans. Atmos. Sci., 42, 321–333, https://doi.org/10.13878/j.cnki.dqkxxb.20190302001, 2019 (in Chinese with English abstract).

Li, X. and He, L.: Analysis of the February 2019 Atmospheric Circulation and Weather, Meteor. Mon., 45, 738–744, 2019 (in Chinese with English abstract).

Li, X., Wang, C., Ling, T., Sun, C., Zhang, Y., and Wang, J.: Features and possible causes of the extreme precipitation anomaly in China during winter 2019/2020, Front. Earth. Sci., 8, 596753, https://doi.org/10.3389/feart.2020.596753, 2020a.

Li, Y., An, W., Pang, H., Wu, S. Y., Tang, Y., Zhang, W., and Hou, S.: Variations of stable isotopic composition in atmospheric water vapor and their controlling factors—A 6-Year continuous sampling study in Nanjing, Eastern China, J. Geophys. Res.-Atmos., 125, e2019JD031697, https://doi.org/10.1029/2019JD031697, 2020b.

Li, X., Wen, Z., and Huang, W.: Modulation of South Asian Jet wave train on the extreme winter precipitation over Southeast China: Comparison between 2015/16 and 2018/19, J. Climate., 33, 4065–4081, https://doi.org/10.1175/JCLI-D-19-0678.1, 2020c.

Merlivat. L. and Jouzel. J.: Global climatic interpretation of the deuterium-oxygen 18 relationship for precipitation, J. Geophys. Res., 84, 5029–5033, https://doi.org/10.1029/JC084iC08p05029, 1979.

Peng, T. R., Wang, C. H., Huang, C. C., Fei, L. Y., Chen, C. T. A., and Hwong, J. L.: Stable isotopic characteristic of Taiwan's precipitation: A case study of western pacific monsoon region, Earth. Planet. Sc. Lett., 289, 357–366, https://doi.org/10.1016/j.epsl.2009.11.024, 2010.

Qin, P., Xie, Z., Zou, J., Liu, S., and Chen, S.: Future precipitation extremes in China under climate change and their physical quantification based on a regional climate model and CMIP5 model simulations, Adv. Atmos. Sci., 38,

300   460−479, https://doi.org/10.1007/s00376-020-0141-4, 2021.

Rahmstorf, S. and Coumou, D.: Increase of extreme events in a warming world, P. Natl. Acad. Sci. USA., 108, 17905−17909, https://doi.org/10.1073/pnas.1101766108, 2011.

Salamalikis, V., Argiriou, A. A., and Dotsika, E.: Stable isotopic composition of atmospheric water vapor in Patras, Greece: A concentration weighted trajectory approach, Atmos. Res., 152, 93−104, https://doi.org/10.1016/j.atmosres.2014.02.021,

305   2015.

Sun, B. and Wang, H.: Analysis of the major atmospheric moisture sources affecting three sub-regions of East China, Int. J. Climatol., 35, 2243–2257, https://doi.org/10.1002/joc.4145, 2015.

Tang, Y., Pang, H., Zhang, W., Li, Y., Wu, S., and Hou, S.: Effects of changes in moisture source and the upstream rainout on stable isotopes in precipitation—A case study in Nanjing, eastern China, Hydrol. Earth. Syst. Sci., 19, 4293−4306,

310   https://doi.org/10.5194/hess-19-4293-2015, 2015.

Tian, L., Yao, T., Macclune, K., White, J., Schilla, A., Vaughn, B., Vachon, R., and Ichiyanagi, K.: Stable isotopic variations in west China: A consideration of moisture sources, J. Geophys. Res.-Atmos., 112, D10112, https://doi.org/10.1029/2006JD007718, 2007.

Uemura, R., Matsui, Y., Yoshimura, K., Motoyama, H., and Yoshida, N.: Evidence of deuterium excess in water vapor as an

315   indicator of ocean surface conditions, J. Geophys. Res.-Atmos., 113, D19114, https://doi.org/10.1029/2008JD010209, 2008.

Wang, B., Wu, R. G., and Fu, X. H.: Pacific-East Asian teleconnection: How does ENSO affect East Asian climate? J. Climate., 13, 1517–1536, https://doi.org/10.1175/1520-0442(2000)013<1517:PEATHD>2.0.CO;2, 2000.

Wang, L. and Feng, J.: Two major modes of the wintertime precipitation over China, Chin. J. Atmos. Sci., 35, 1105−1116,

320   https://doi.org/10.3878/j.issn.1006-9895.2011.06.10, 2011 (in Chinese with English abstract).

Wang, S., Zhang, M., Crawford, J., Hughes, C. E., Du, M., and Liu, X.: The effect of moisture source and synoptic conditions on precipitation isotopes in arid central Asia, J. Geophys. Res.-Atmos., 122, 2667–2682, https://doi.org/10.1002/2015JD024626, 2017.

Wang, Z., Sun, J., Wu, J., Ning, F., and Chen, W.: Attribution of persistent precipitation in the Yangtze-Huaihe river basin
   during February 2019, Adv. Atmos. Sci., 37, 1389–1404, https://doi.org/10.1007/s00376-020-0107-6, 2020.

Xu, R., Zhang, T., Rao, X., and You, Y.: Analysis of the December 2018 Atmospheric Circulation and Weather, Meteor. Mon.,
   45, 437–444, 2019 (in Chinese with English abstract).

Yang, Z., Huang, W., He, X., Wang, Y., Qiu, T., Wright, J. S., and Wang, B.: Synoptic conditions and moisture sources for
   extreme snowfall events over East China, J. Geophys. Res.-Atmos., 124, 601–623,
   https://doi.org/10.1029/2018JD029280, 2019.

Yao, T., Zhang, X., Guan, H., Zhou, H., Hua, M., and Wang, X.: Climatic and environmental controls on stable isotopes in
   atmospheric water vapor near the surface observed in Changsha, China, Atmos. Environ., 189, 252−263,
   https://doi.org/10.1016/j.atmosenv.2018.07.008, 2018.

Yao, Y., Lin, H., and Wu, Q.: Subseasonal variability of precipitation in China during boreal winter, J. Climate., 28, 6548–
   6559, https://doi.org/10.1175/JCLI-D-15-0033.1, 2015.

Yu, W., Tian, L., Ma, Y., Xu, B., and Qu, D.: Simultaneous monitoring of stable oxygen isotope composition in water vapour
   and precipitation over the central Tibetan Plateau, Atmos. Chem. Phys., 15, 10251–10262,
   https://doi.org/10.5194/acp-15-10251-2015, 2015.

Zhao, Y., Gui, H., Li, S., and You, Y.: Analysis of the January 2019 Atmospheric Circulation and Weather, Meteor. Mon., 45,
   587–592, 2019 (in Chinese with English abstract).

Zhao, N., Manda, A., Guo, X., Kikuchi, K., Nasuno, T., Nakano, M., Zhang, Y., and Wang, B.: A Lagrangian view of
   moisture transport related to the heavy rainfall of July 2020 in Japan: Importance of the moistening over the subtropical
   regions, Geophys. Res. Lett., 48, e2020GL091441, https://doi.org/10.1029/2020GL091441, 2021.

Zhou, B., Gu, L., Ding, Y., Shao, L., Wu, Z., Yang, X., Li, C., Li, Z., Wang, X., Cao, Y., Zeng, B., Yu, M., Wang, M., Wang,
   S., Sun, H., Duan, A., An, Y., Wang, X., and Kong, W.: The great 2008 Chinese ice storm: Its socioeconomic-ecological
   impact and sustainability lessons learned, B. Am. Meteorol. Soc., 92, 47–60, https://doi.org/10.1175/2010BAMS2857.1,
   2011.

Zhou, J. and Li, T.: A tentative study of the relationship between annual δ^{18}O & δD variations of precipitation and atmospheric circulations—A case from Southwest China, Quatern. Int., 479, 117–127,
350   https://doi.org/10.1016/j.quaint.2017.05.038, 2017.

Zhou, L., Tam, C. Y., Zhou, W., and Chan, J. C. L.: Influence of South China Sea SST and the ENSO on winter rainfall over South China, Adv. Atmos. Sci., 27, 832–844, https://doi.org/10.1007/s00376-009-9102-7, 2010.

Zong, H., Bueh, C., Ji, L.: Wintertime extreme precipitation event over southern China and its typical circulation features. Chinese. Sci. Bull., 59, 1036–1044, https://doi.org/10.1007/s11434-014-0124-x, 2014.
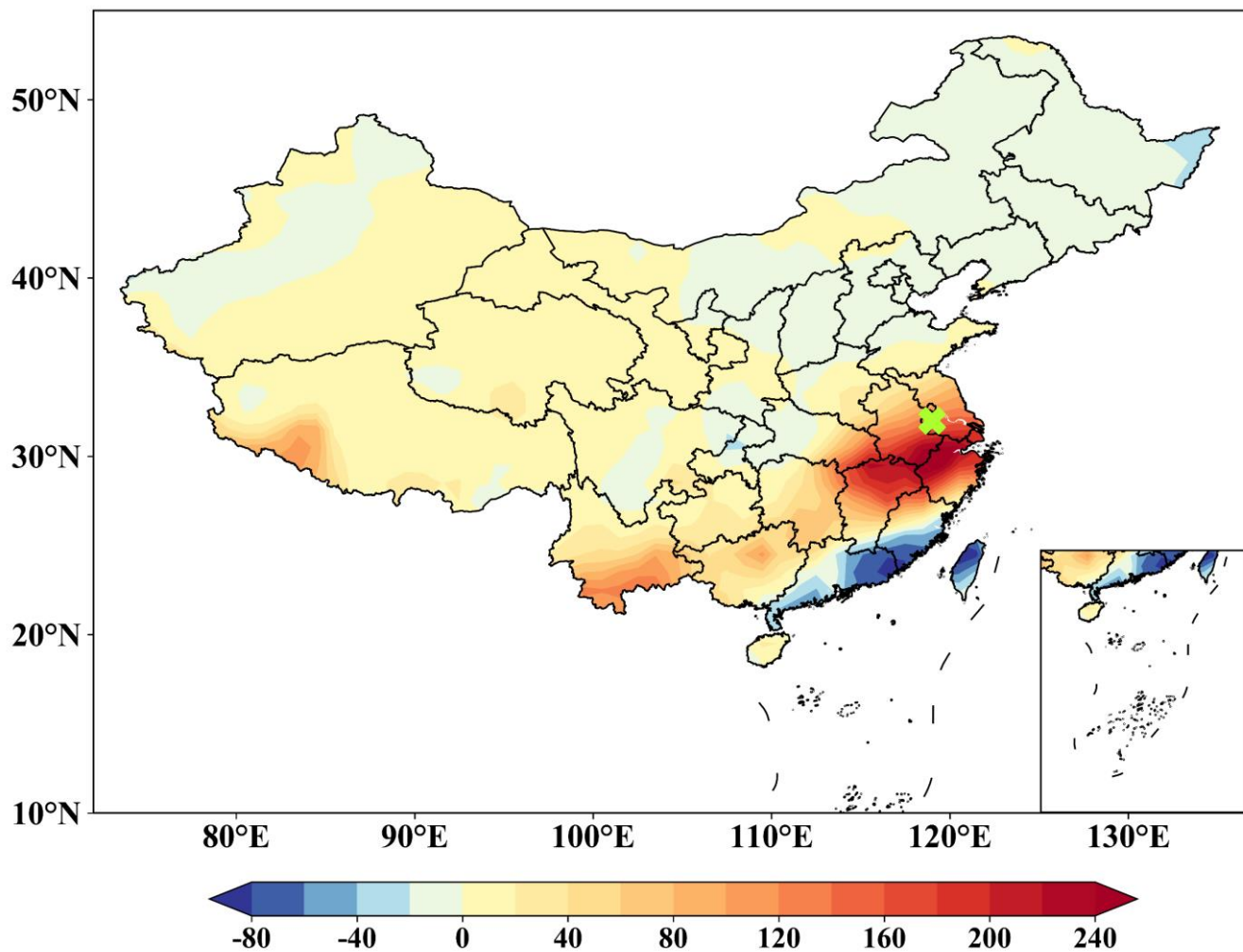
355

Fig 1. Winter (December–February) precipitation anomalies (shading; units: mm) over China in the winter of 2018/2019. "X" represents the sampling site at Nanjing. The anomalies were calculated with respect to the 1981–2010 climatology.
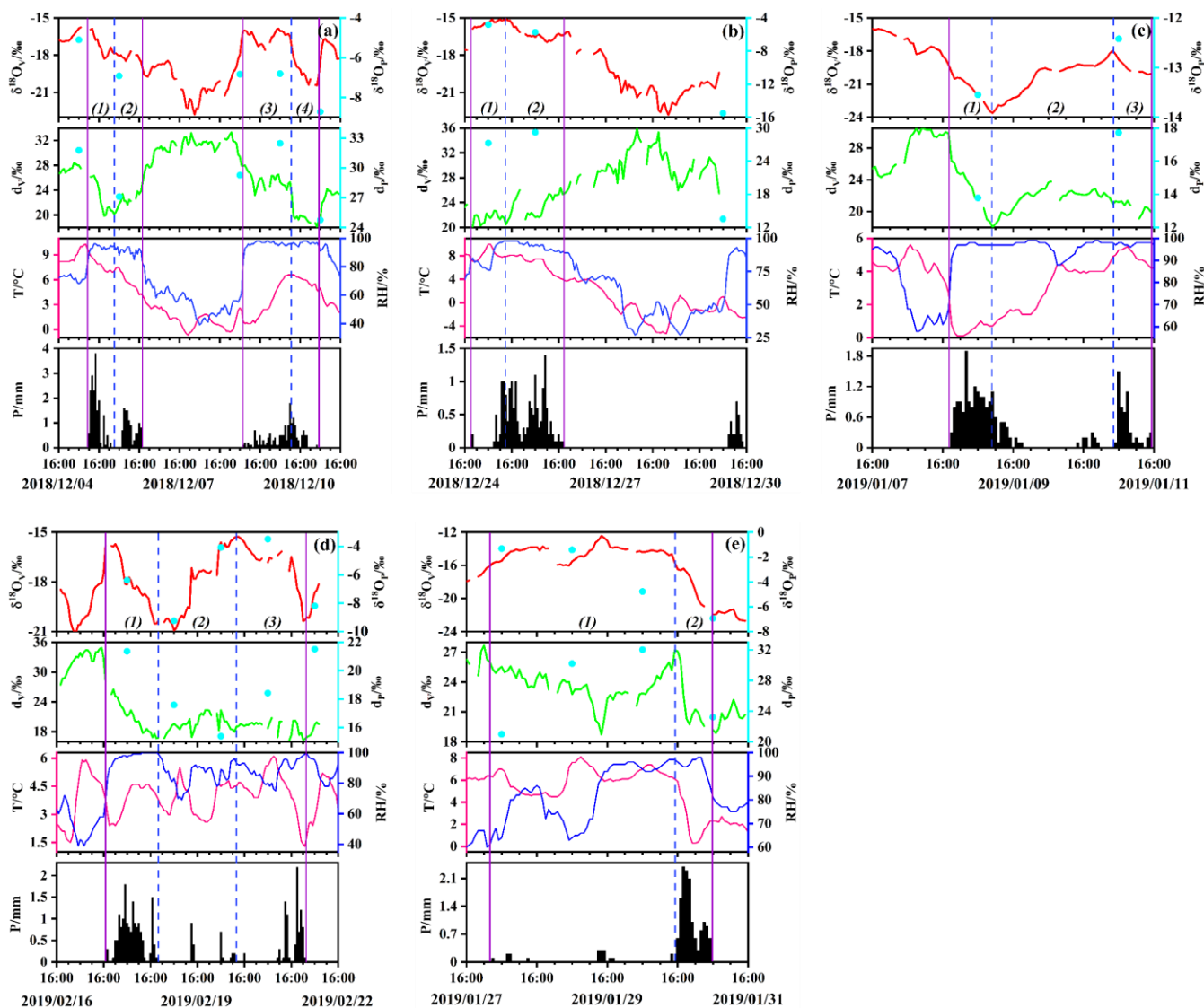
Fig 2. Time series of hourly water vapor $\delta^{18}O_v$ and d_v, daily precipitation $\delta^{18}O_p$ and d_p (cyan dots), air temperature (T), relative
360   **humidity (RH), and precipitation amount (P) at Nanjing. (a) Event December 4−11, 2018; (b) Event December 24−30, 2018; (c)**
Event January 7−11, 2019; (d) Event February 16−22, 2019; (e) Event January 27−31, 2019. The vertical purple lines and blue
dashed lines indicate the concentrated rainfall period and different stages of each precipitation event, respectively.
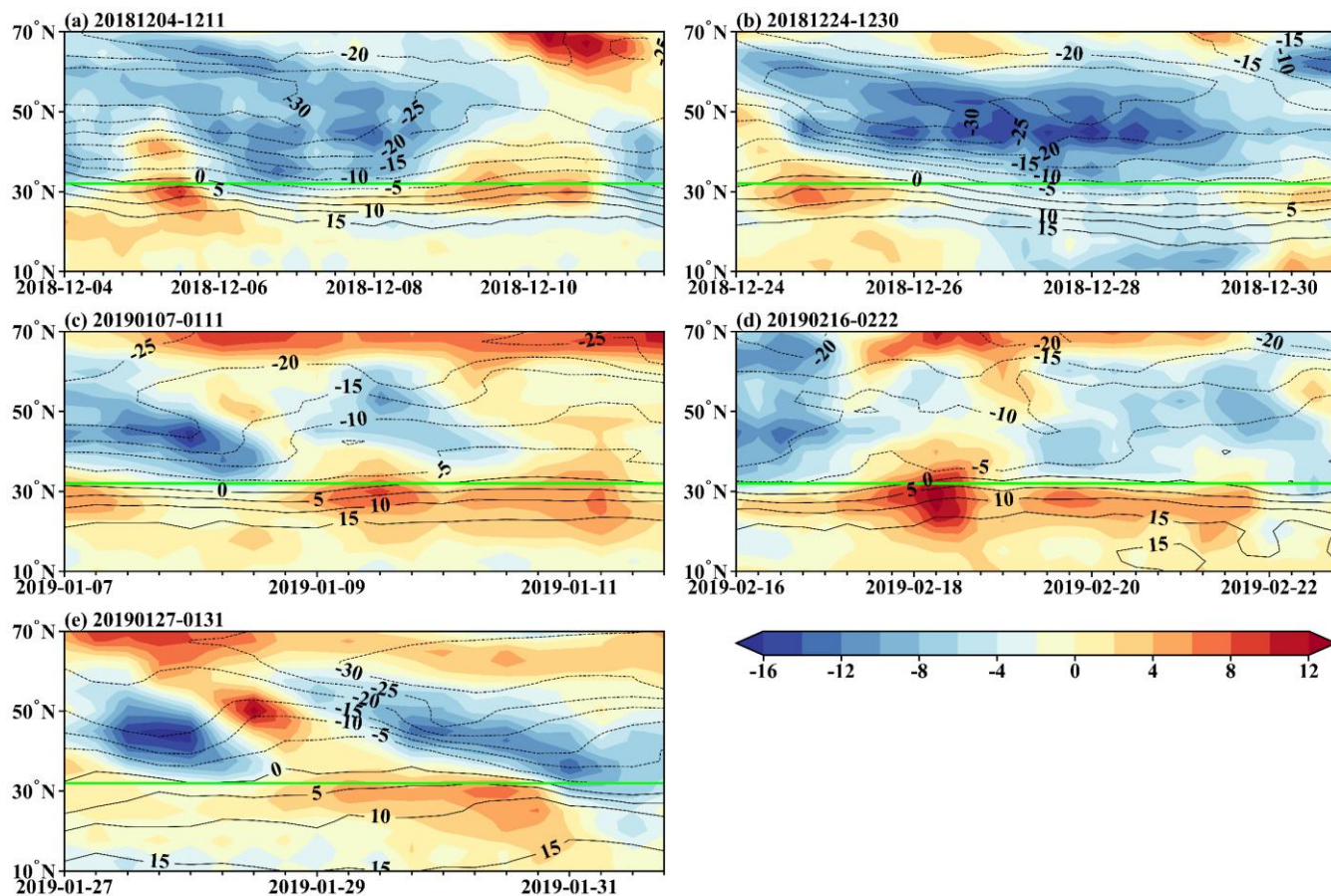
Fig 3. Latitude-time cross section of the meridional wind component (shading; units: m/s) and temperature (contour; units: °C) at
365 **850 hPa along the 120°E. The horizontal green lines indicate the latitude of the sampling site at Nanjing (32.12°N).**
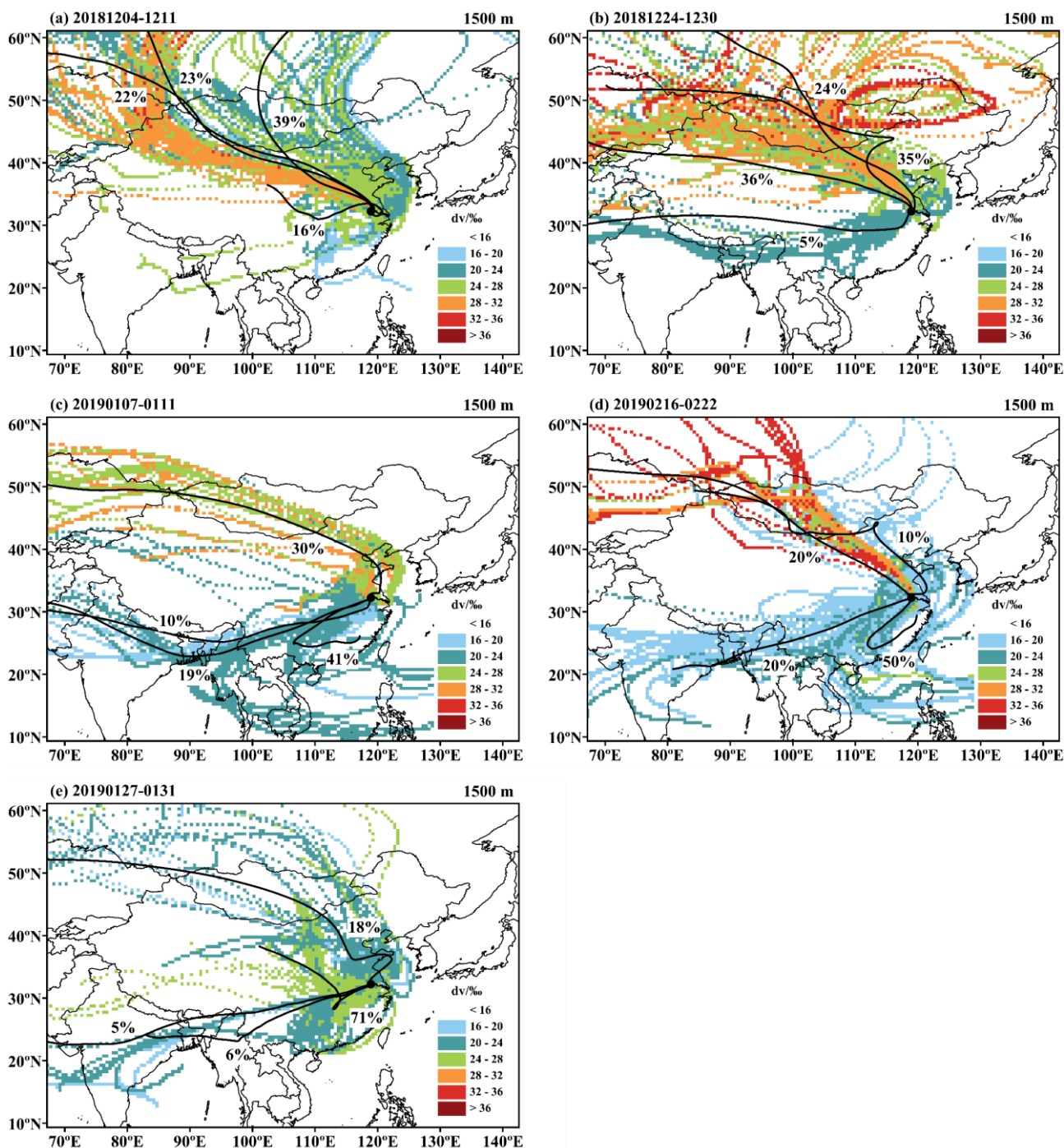
Fig 4. Concentration field of water vapor d_v for 192 h HYSPLIT back trajectories and clusters for the five typical precipitation events. The black circle indicates the location of Nanjing.
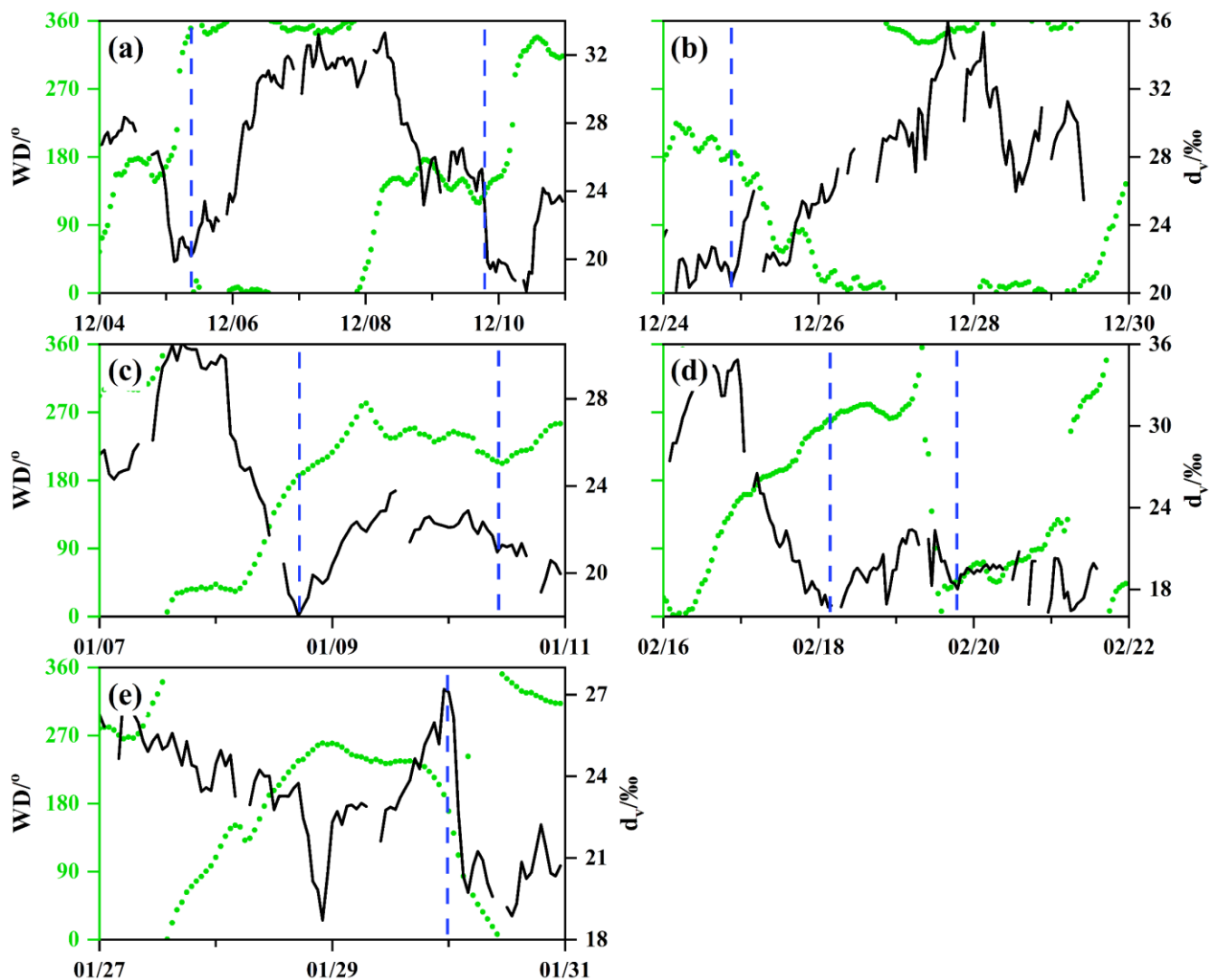
Fig 5. Time series of hourly water vapor d$_v$ (black lines) and 850 hPa wind direction (green dots) of precipitation events. The vertical blue dashed lines indicate the different stages of precipitation events. (a) Event December 4−11, 2018; (b) Event December 24−30, 2018; (c) Event January 7−11, 2019; (d) Event February 16−22, 2019; (e) Event January 27−31, 2019.